Journal of Sound and Vibration (2003) **259**(2), 387–407
doi:10.1006/jsvi.2002.5334, available online at http://www.idealibrary.com on IDEAL®

INPUT FORCES ESTIMATION OF BEAM STRUCTURES BY AN INVERSE METHOD

C.-K. Ma

Department of Naval Architecture and Marine Engineering, Chung-Cheng Institute of Technology, Ta-Hsi, Tao-Yuan, 33509*, Taiwan, Republic of China E-mail: chihkao@ccit.edu.tw*

J.-M. Chang

Department of System Engineering, Chung-Cheng Institute of Technology, Ta-Hsi, Tao-Yuan 33509*, Taiwan, Republic of China*

AND

D.-C. Lin

Department of Industry Management, Diwan College of Management, Matou, Tainan 721*, Taiwan, Republic of China*

(*Received* 2 *July* 2001, *and in final form* 2 *April* 2002)

An on-line recursive inverse method to estimate the input forces of beam structures is presented. The inverse method is based on the Kalman filter and a recursive least-squares algorithm. The filter models the system dynamics in a linear set of state equations. The state equations of the beam structures were constructed using the finite element method. The practicability and accuracy of the estimation method were examined with numerical simulations from which the input forces of a cantilever beam with a lumped mass on the free end were estimated from the output responses. In the numerical experiments, the cantilever beam was subjected to five types of input forces, i.e., sinusoidal, triangular impulse, rectangular impulse, a series of impulses and random. The simulation results show that the inverse method has an excellent performance to estimate the input forces of beam structural systems from the noisy measurements.

1. INTRODUCTION

The determination of excitation forces is a very important task in structure design. However, direct measurements of the excitation forces are not always feasible, e.g., excitations of wind, seismic, explosion and shock. As a result, an indirect estimation for the excitation forces is frequently employed. For the input forces estimation problems, Stevens [1] has presented an overview of the force identification process for the case of linear vibration systems. Hillary and Ewins [2] investigated the problems of sinusoidal loads identification of a cantilever beam and determination of impact forces on aircraft engine turbine blades with a least-squares method. Öry *et al.* [3] used the William's method [4] with a time integration scheme to identify the shock loading applied on a beam. Bateman *et al.* [5] presented two force reconstruction techniques, i.e., the sum of weighted acceleration and the deconvolution, to evaluate the impact test for a nuclear transportation cask. Doyle [6–10] has developed many force estimation methods to

0022-460X/02/$35.00

identify the impact loads of composite beams and plates. Michaels and Pao [11] presented a deconvolution method, which was applied to determine the orientation and time-dependent amplitude of the input force from the transient response of a plate. Johnson [12] presented the characteristic dynamical behavior of a linear system that was modelled by a state variable model, involving input-derivative terms, and used the deconvolution approach to identify the input forces/moments. More recently, Huang [13] used an algorithm based on the conjugate gradient method to estimate the unknown external forces in the inverse non-linear force vibration problems.

In the previous study [14], we have presented an inverse method to estimate impulsive loads on lumped-mass structural systems. The inverse method is based on the Kalman filter and a recursive least-squares method. The simulation results indicate that the method can accurately estimate unknown impulsive loads. In addition, we have developed an experimental apparatus and conducted a series of experiments on a physical cantilever beam to identify the excitation forces [15]. The estimation results have demonstrated the validity of the estimation method. However, the state-space model of the beam was simplified to a single-degree-of-freedom lumped-mass system.

In the present work, the input forces estimation method [14] is applied in the beam structural systems. We first used the finite element method (FEM) to construct the system state equations of the beam structures, and then established an estimation scheme to determine the unknown excitation forces. The practicability of the estimation method was verified with numerical simulations of a cantilever beam. The cantilever beam with a lumped mass mounted on the free end was subjected to five types of input forces, i.e., sinusoidal, triangular and rectangular impulses, a series of impulses and random. The input forces were estimated from the simulated noisy responses through the input estimation algorithm. The estimated input forces were compared with the exact input forces to demonstrate the accuracy of the inverse method.

2. PROBLEM FORMULATION

2.1. STATE EQUATIONS OF THE SYSTEM

The Kalman filter, which comprises two parts (i.e., prediction and correction), is based on the state-space analysis method. In the present study, we used the FEM to construct the state-space model of beam structural systems. The finite element model of a beam structure is considered to be an "n"-degrees-of-freedom system. Therefore, the differential equations of motion of the system in terms of mass, stiffness and damping matrices are

$$\mathbf{M}\ddot{\mathbf{Y}}(t) + \mathbf{C}\dot{\mathbf{Y}}(t) + \mathbf{K}\mathbf{Y}(t) = \mathbf{F}(t), \tag{1}$$

where $\mathbf{M}$ denotes the $n \times n$ mass matrix, $\mathbf{C}$ the $n \times n$ damping matrix, $\mathbf{K}$ the $n \times n$ stiffness matrix, $\mathbf{F}(t)$ the $n \times 1$ input force vector, and $\ddot{\mathbf{Y}}(t)$, $\dot{\mathbf{Y}}(t)$ and $\mathbf{Y}(t)$ denotes the $n \times 1$ vectors of acceleration, velocity and displacement respectively. The matrices $\mathbf{M}$ and $\mathbf{K}$ were obtained from the FEM. The matrix $\mathbf{C}$ was obtained by assembling the matrices $\mathbf{M}$ and $\mathbf{K}$ as a proportional damping model.

In converting to the state-space model, the state variables of the second order dynamic system with n degrees of freedom are represented by a $2n \times 1$ state vector, i.e., $\mathbf{X}(t) = [\mathbf{Y}(t)\dot{\mathbf{Y}}(t)]^{\mathrm{T}}$. From equation (1), the continuous-time state equations and measurement equations can be written as

$$\dot{\mathbf{X}}(t) = \mathbf{A}\mathbf{X}(t) + \mathbf{B}\mathbf{F}(t), \tag{2}$$

$$\mathbf{Z}(t) = \mathbf{H}\mathbf{X}(t), \tag{3}$$

where

$$\mathbf{A} = \begin{bmatrix} \mathbf{0}_{n\times n} & \mathbf{I}_{n\times n} \\ -\mathbf{M}^{-1}\mathbf{K} & -\mathbf{M}^{-1}\mathbf{C} \end{bmatrix}, \quad \mathbf{B} = \begin{bmatrix} \mathbf{0}_{n\times n} \\ \mathbf{M}^{-1} \end{bmatrix},$$

$\mathbf{X}(t) = [X_1(t)X_2(t)\ldots X_{2n-1}(t)X_{2n}(t)]^{\mathrm{T}}$, $\mathbf{F}(t) = [F_1 \ F_2 \ F_3 \ \ldots \ F_n]^{\mathrm{T}}$, $\mathbf{H} = \mathbf{I}_{2n\times 2n}$ is the measurement matrix and $\mathbf{Z}(t)$ represents the observation vector.

Equations (2) and (3) are discretized over time intervals of length Δt, and associated with process noise input [16], i.e., the statistical description of the system noise and uncertainty in the dynamic models. Then, equation (2) becomes

$$\begin{aligned} \mathbf{X}(k+1) &= \Phi\mathbf{X}(k) + \Gamma[\mathbf{F}(k) + \mathbf{w}(k)], \\ \mathbf{X}(k) &= [X_1(k) \ X_2(k) \ \cdots \ X_{2n-1}(k) \ X_{2n}(k)]^{\mathrm{T}}, \\ \Phi &= \exp(\mathbf{A}\,\Delta t), \\ \Gamma &= \int_{k\,\Delta t}^{(k+1)\Delta t} \exp\{\mathbf{A}[(k+1)\Delta t - \tau]\}\mathbf{B}\,\mathrm{d}\tau, \\ \mathbf{w}(k) &= [w_1(k) \ w_2(k) \ \ldots \ w_n(k)]^{\mathrm{T}}, \\ \mathbf{F}(k) &= [F_1(k) \ F_2(k) \ \ldots \ F_n(k)]^{\mathrm{T}}, \end{aligned} \tag{4}$$

where $\mathbf{X}(k)$ represents the state vector, Φ the state transition matrix, Γ the input matrix, Δt the sampling interval, $\mathbf{F}(k)$ the sequence of deterministic input and $\mathbf{w}(k)$ the noise vector which is assumed to be zero mean and white with variance $E\{\mathbf{w}(k)\mathbf{w}^T(j)\} = \mathbf{Q}\delta_{kj}$, $\mathbf{Q} = Q_W \times \mathbf{I}_{2n\times 2n}$, here $\mathbf{Q}$ is the process noise covariance matrix and δ_{kj} is the Kronecker delta.

In order to consider the measurement noise, Equation (3) is expressed as

$$\begin{aligned} \mathbf{Z}(\mathrm{k}) &= \mathbf{H}\mathbf{X}(k) + \mathbf{v}(k), \\ \mathbf{Z}(k) &= [Z_1(k) \ Z_2(k) \ Z_3(k) \ \cdots \ Z_{2n}(k)]^{\mathrm{T}}, \\ \mathbf{v}(k) &= [v_1(k) \ v_2(k) \ v_3(k)\cdots v_{2n}(k)]^{\mathrm{T}}, \end{aligned} \tag{5}$$

where $\mathbf{v}(k)$ represents the measurement noise vector. Also, $\mathbf{v}(k)$ is assumed to be zero mean and white noise. The variance of $\mathbf{v}(k)$ is given by $E\{\mathbf{v}(k)\mathbf{v}^{\mathrm{T}}(j)\} = \mathbf{R}\delta_{kj}$, $\mathbf{R} = R_v \times \mathbf{I}_{2n\times 2n}$ and $R_v = \sigma^2$, here $\mathbf{R}$ is the measurement noise covariance matrix and σ represents the standard deviation of measurement noise.

2.2. RECURSIVE INPUT ESTIMATION APPROACH

Input force estimation is a process of determining the applied loadings from the measurements of the system responses. The present input estimation method consists of two parts: the Kalman filter and an estimator. The Kalman filter is used to generate the residual innovation sequence. The estimator then computes the onset time histories of the excitation forces by utilizing the residual innovation sequence through a recursive least-squares algorithm. The detailed derivation of this technique can be found in the appendix of Tuan *et al.* [17].

The equations of the Kalman filter are

$$\bar{\mathbf{X}}(k/k-1) = \Phi\bar{\mathbf{X}}(k-1/k-1) \tag{6}$$

$$\mathbf{P}(k/k-1) = \Phi\mathbf{P}(k-1/k-1)\Phi^{\mathrm{T}} + \Gamma\mathbf{Q}\Gamma^{\mathrm{T}}, \tag{7}$$

$$\mathbf{S}(k) = \mathbf{H}\mathbf{P}(k/k-1)\mathbf{H}^{\mathrm{T}} + \mathbf{R}, \tag{8}$$

$$\mathbf{K}_a(k) = \mathbf{P}(k/k-1)\mathbf{H}^{\mathrm{T}}\mathbf{S}^{-1}(k), \tag{9}$$

$$\mathbf{P}(k/k) = [\mathbf{I} - \mathbf{K}_a(k)\mathbf{H}]\mathbf{P}(k/k-1), \tag{10}$$

$$\bar{\mathbf{Z}}(k) = \mathbf{Z}(k) - \mathbf{H}\bar{\mathbf{X}}(k/k-1), \tag{11}$$

$$\bar{\mathbf{X}}(k/k) = \bar{\mathbf{X}}(k/k-1) + \mathbf{K}_a(k)\bar{\mathbf{Z}}(k). \tag{12}$$

The equations of the recursive least-squares algorithm are

$$\mathbf{B}_s(k) = \mathbf{H}[\Phi\mathbf{M}_s(k-1) + \mathbf{I}]\Gamma, \tag{13}$$

$$\mathbf{M}_s(k) = [\mathbf{I}\text{-}\mathbf{K}_a(k)\mathbf{H}][\Phi\mathbf{M}_s(k-1) + \mathbf{I}], \tag{14}$$

$$\mathbf{K}_b(k) = \gamma^{-1}\mathbf{P}_b(k-1)\mathbf{B}_s^{\mathrm{T}}(k)[\mathbf{B}_s(k)\gamma^{-1}\mathbf{P}_b(k-1)\mathbf{B}_s^{\mathrm{T}}(k) + \mathbf{S}(k)]^{-1}, \tag{15}$$

$$\mathbf{P}_b(k) = [\mathbf{I} - \mathbf{K}_b(k)\mathbf{B}_s(k)]\gamma^{-1}\mathbf{P}_b(k-1), \tag{16}$$

$$\hat{\mathbf{F}}(k) = \hat{\mathbf{F}}(k-1) + \mathbf{K}_b(k)[\bar{\mathbf{Z}}(k) - \mathbf{B}_s(k)\hat{\mathbf{F}}(k-1)], \tag{17}$$

where $\mathbf{P}$ denotes the filter's error covariance matrix, $\mathbf{S}(k)$ represents the innovation covariance, $\mathbf{K}_a(k)$ is the Kalman gain, $\mathbf{B}_s(k)$ and $\mathbf{M}_s(k)$ are the sensitivity matrices, $\bar{\mathbf{Z}}(k)$ is the innovation, $\mathbf{K}_b(k)$ is the correction gain for the updating $\hat{\mathbf{F}}(k)$ and $\mathbf{P}_b$ represents the error covariance of the estimated input vector $\hat{\mathbf{F}}(k)$. The scalar parameter γ, i.e., fading factors, is employed in the present algorithm to compromise between the fast adaptive capability and the loss of estimate accuracy.

The procedure to estimate the unknown input forces using the inverse method is summarized as follows:

(1) Derive and identify the system state-space model, i.e., equations (4) and (5), and measure the system responses $\mathbf{X}(k)$.

(2) Use the Kalman filter equations, i.e., equations (6)–(12), to obtain the innovation covariance $\mathbf{S}(k)$, innovation $\bar{\mathbf{Z}}(k)$ and Kalman gain $\mathbf{K}_a(k)$.

(3) Use the recursive least-squares algorithm, i.e., equations (13)–(17), to estimate the unknown input forces $\hat{\mathbf{F}}(k)$.

3. NUMERICAL SIMULATIONS AND RESULTS

To illustrate the practicability and accuracy of the present approach in estimating unknown input forces, numerical experiments of a cantilever beam [15] are investigated here. The finite element model of the cantilever beam with a lumped mass on the free end is shown in Figure 1. The material data and dimensions of the beam and lumped mass are given in Table 1. The element mass matrix $\mathbf{M}^e$ and element stiffness matrix $\mathbf{K}^e$ of the beam are as follows [18]:

$$\mathbf{M}^e = \frac{\rho_s \ell}{420}\begin{bmatrix} 156 & 22\ell & 54 & -13\ell \\ & 4\ell^2 & 13\ell & -3\ell^2 \\ & & 156 & -22\ell \\ SYM & & & 4\ell^2 \end{bmatrix}$$

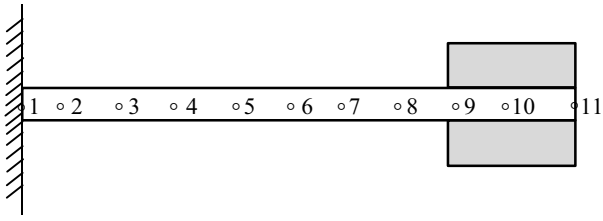

Figure 1. Finite element model of the cantilever beam with a lumped mass mounted on the free end (10 elements with 11 nodes).

TABLE 1

The Material data and dimensions of the cantilever beam and lumped mass

	Beam	Lumped mass
Material	Aluminum alloy	Brass
Density (kg/m^3)	2710	8400
Elastic modulus (Gpa)	70	100
The Poisson ratio	0·33	0·34
Length (m)	0·264	0·020
Width (m)	0·030	0·030
Height (m)	0·005	0·040

and

$$\mathbf{K}^e = \frac{EI_s}{\ell^3}\begin{bmatrix} 12 & 6\ell & -12 & 6\ell \\ & 4\ell^2 & -6\ell & 2\ell^2 \\ & & 12 & -6\ell \\ SYM & & & 4\ell^2 \end{bmatrix},$$

where ρ_s is the mass per unit length of the beam, ℓ the length of the beam element, E the elastic modulus and I_s the moment of inertia of the cross-section. The global matrices $\mathbf{M}$ and $\mathbf{K}$ of the beam were obtained by assembling the matrices $\mathbf{M}^e$ and $\mathbf{K}^e$. The proportional damping matrix $\mathbf{C}$ was expressed as below:

$$\mathbf{C} = \alpha\mathbf{M} + \beta\mathbf{K},$$

where α and β are constants with proper units. A comparison of the FEM and experimentally estimated natural frequencies for the first three modes of the cantilever beam is shown in Table 2.

Five types of input forces were considered in the numerical experiments, i.e., sinusoidal, triangular impulse, rectangular impulse, a series of impulses and random. The simulated measurements of the cantilever beam were loaded into the inverse estimation algorithm, i.e., equations (7)–(17), to identify the corresponding input forces.

TABLE 2

Comparison of FEM and experimental results of the natural frequencies

Mode	FEM (Hz)	Experiment [15] (Hz)
1	17·92	17·45
2	223·88	215·34
3	558·54	560·74

3.1. ESTIMATION OF TWO SINUSOIDAL FORCES

In the first numerical experiment, two sinusoidal forces were introduced as below:

$$F_{10}(t) = 2 \times \sin(180\pi t) + 1 \times \sin(90\pi \mathrm{t})\ (\mathrm{N}),$$
$$F_7(\mathrm{t}) = 1 \times \sin(180\pi t)\ (\mathrm{N}).$$

The two sinusoidal forces acted on nodes 10 and 7 of the beam. The dynamic responses of the beam were solved by using a numerical method. The parameters used in the numerical experiment are given as follows: null initial conditions, sampling interval $\Delta t = 1 \times 10^{-4}$ s, fading factor $\gamma = 0.69$, covariance matrix of process noise $\mathbf{Q} = Q_w \times \mathbf{I}_{n\times n}$, $Q_w = 1 \times 10^{-9}$, covariance matrix of measurement noise $\mathbf{R} = R_v \times \mathbf{I}_{2n\times 2n}$, $R_v = 1 \times 10^{-15}$. The input forces estimation was first performed by using the errorless measurement data (see Table 3). Figure 2 shows the displacements at nodes 10, 8 and 7 of the cantilever beam. The exact and estimated input forces are shown in Figure 3. The figure also illustrates the estimation result of node 8 where no input force was applied. The estimation results have demonstrated the validity of the present inverse estimation algorithm. Next, the influence of the process and measurement noises on the estimation results was considered. The displacements with assuming process and measurement noises of the cantilever beam are depicted in Figure 4 (solid line indicates the exact displacement, dotted line the contaminated displacement). The estimation results of the two sinusoidal forces are shown in Figure 5. The error used to quantify the deviations between the estimated and exact input forces was defined as below [19]:

$$Error\ (\%) \frac{\sqrt{\sum_{i=1}^{p} [f^{ex}(t_i) - f^{es}(t_i)]^2}}{\sqrt{\sum_{i=1}^{p} [f^{ex}(t_i)]^2}} \times 100,$$

where $f^{ex}(t_i)$ and $f^{es}(t_i)$ designate the exact and estimated forces at time t_i respectively.

Because large process and measurement noise covariances are considered, the errors of the two estimated sinusoidal forces are relatively high (17·57 and 9·29%). However, the

TABLE 3

Errors of the estimated input forces at different levels of Q_w and R_v

	$Q_w = 1 \times 10^{-9}$, $R_v = 1 \times 10^{-15}$	$Q_w = 1 \times 10^{-10}$, $R_v = 1 \times 10^{-16}$
Two sinusoidal forces	17·57% and 9·29%	7·38% and 3·08%
Triangular impulse	16·83%	8·58%
Rectangular impulse	14·80%	9·89%
A series of impulses	32·51%	20·42%
Random force	—	—

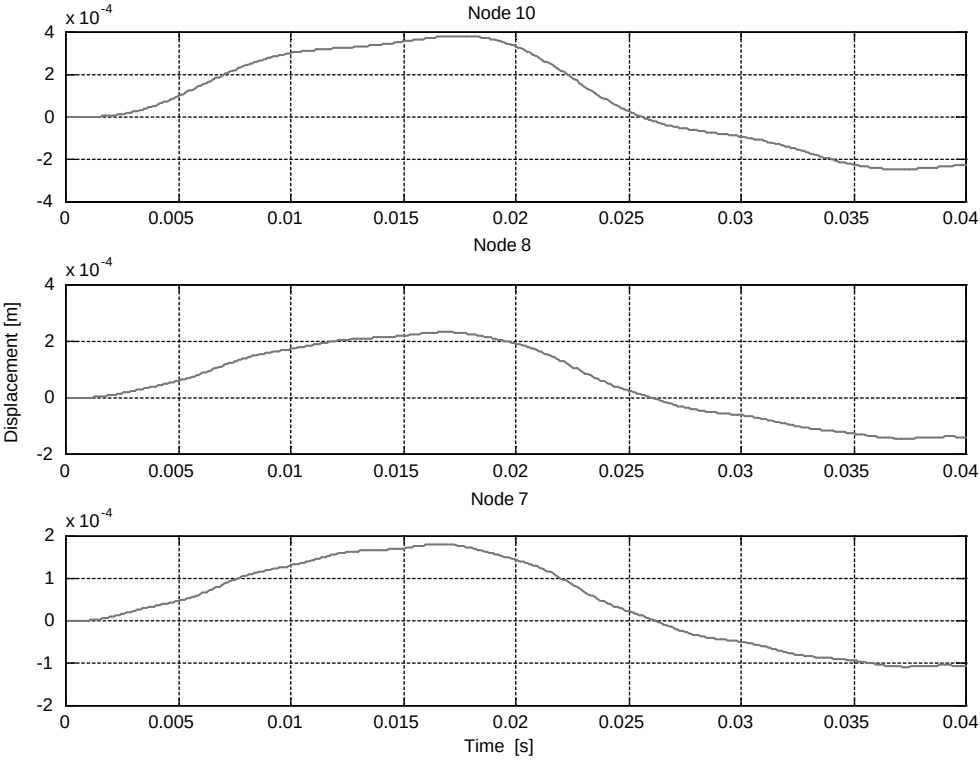

Figure 2. Time histories of the displacements at nodes 10, 8 and 7.

present inverse method still has the tracking capability to identify the two sinusoidal forces. To obtain better estimation results, we adjusted the values of $Q_w = 1 \times 10^{-10}$ and $R_v = 1 \times 10^{-16}$. Figures 6 and 7 depict the corresponding time histories of the displacements and estimation results. The results reveal a very good estimating ability, and the errors of the two estimated sinusoidal forces reduce obviously (7·38 and 3·08%).

3.2. ESTIMATION OF A TRIANGULAR IMPULSE

In the second test case, a triangular impulse that acted on node 10 was expressed as

$$F_{10}(t) = 4t/(5 \times 10^{-3})(\mathrm{N}), \quad 0 \leqslant t \leqslant 0{\cdot}005\ (\mathrm{s}),$$

$$F_{10}(t) = 4(0{\cdot}01 - t)/(5 \times 10^{-3})\ (\mathrm{N}), \quad 0{\cdot}005 < t \leqslant 0{\cdot}010\ (\mathrm{s}),$$

$$F_{10}(t) = 0\ (\mathrm{N}), \quad t > 0{\cdot}010\ (\mathrm{s}).$$

The simulation parameters are given by null initial conditions, $\Delta t = 1 \times 10^{-4}$ s, $\gamma = 0.52$, $Q_w = 1 \times 10^{-9}$, $R_v = 1 \times 10^{-15}$. Figures 8 and 9 depict the time histories of the displacement and estimation result of the triangular impulse (see also Figure 10). The error of the estimated triangular impulse is 16.83%. With reference to Figure 11, we learned that the selection of small values of process and measurement noise covariances, i.e., $Q_w = 1 \times 10^{-10}$ and $R_v = 1 \times 10^{-16}$, can provide a better estimation result of the triangular impulse. The error of the estimation result reduces to 8.58%.

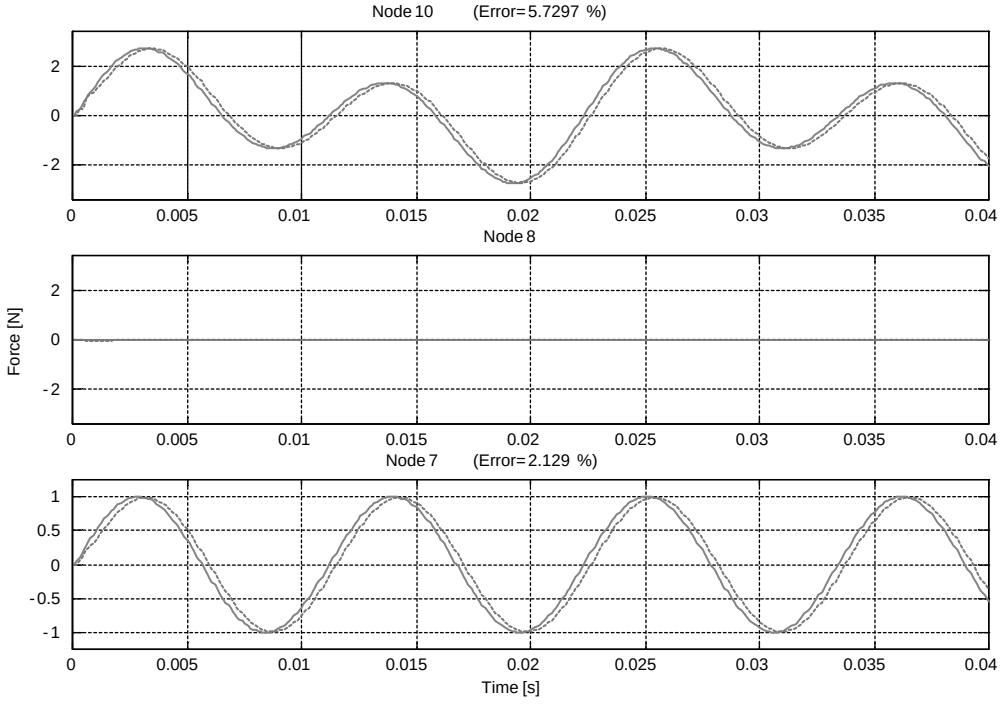

Figure 3. Time histories of the sinusoidal forces at nodes 10, 8 and 7: (—) exact; (- - -) estimated; $\gamma = 0{\cdot}69$, $Q_w = 1 \times 10^{-9}$, $R_v = 1 \times 10^{-15}$.

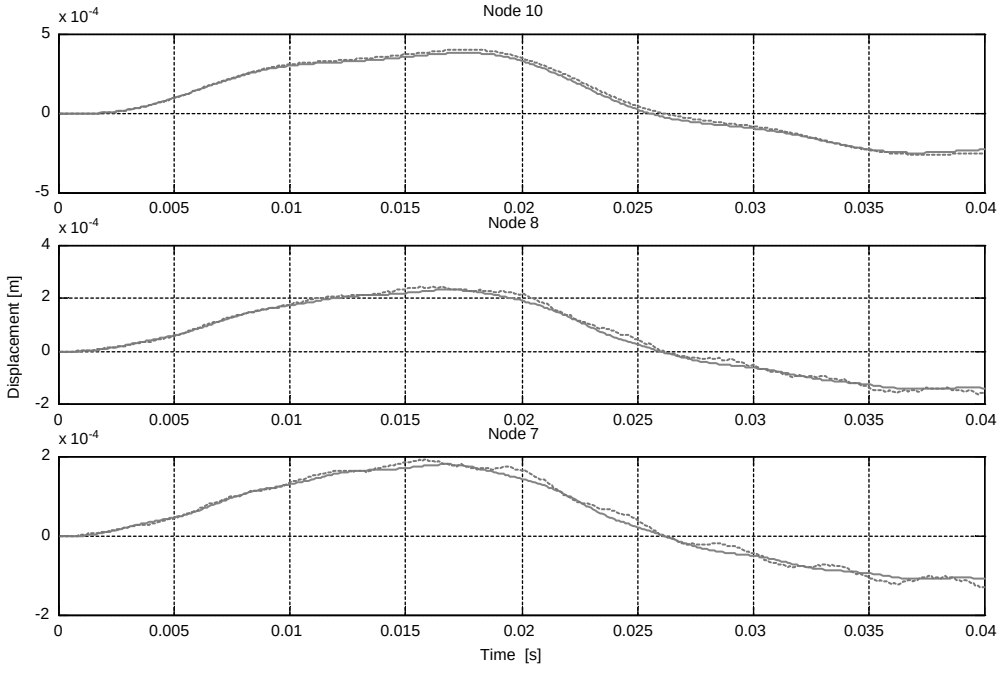

Figure 4. Time histories of the displacements at nodes 10, 8 and 7: (—) exact; (- - -) contaminative; $Q_w = 1 \times 10^{-9}$, $R_v = 1 \times 10^{-15}$.

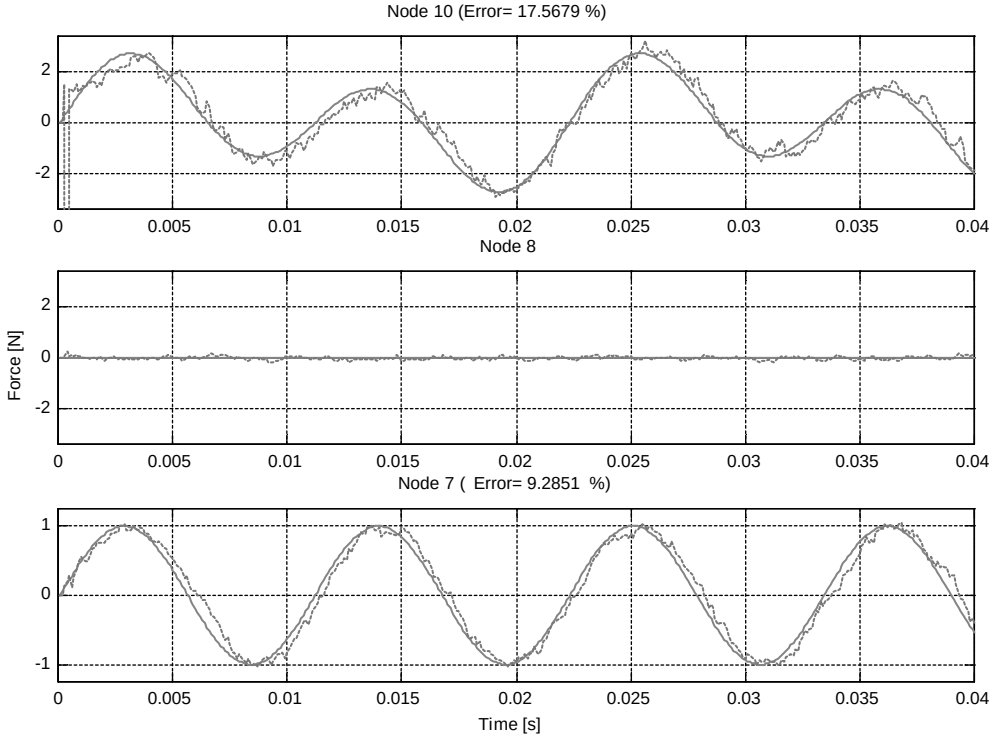

Figure 5. Time histories of the sinusoidal forces at nodes 10, 8 and 7: (—) exact; (- - -) estimated; $\gamma = 0{\cdot}69$, $Q_w = 1 \times 10^{-9}$, $R_v = 1 \times 10^{-15}$.

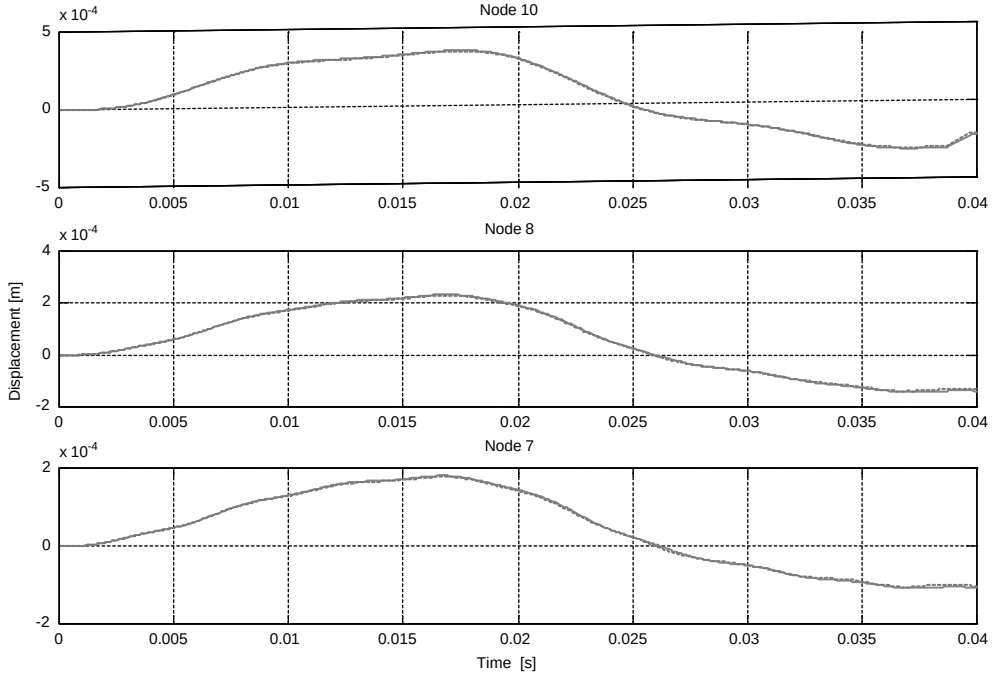

Figure 6. Time histories of the displacements at nodes 10, 8 and 7. (—) exact; (- - -) contaminative; $Q_w = 1 \times 10^{-10}$, $R_v = 1 \times 10^{-16}$.

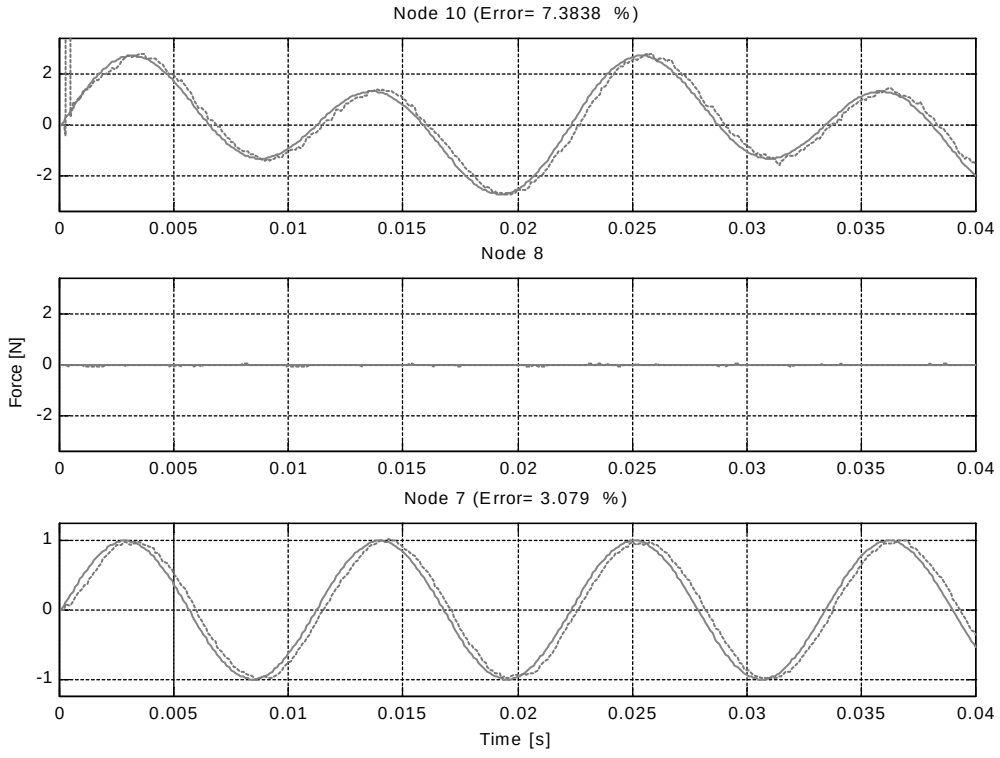

Figure 7. Time histories of the sinusoidal forces at nodes 10, 8 and 7: (—) exact; (- - -) estimated; $\gamma = 0{\cdot}69$, $Q_w = 1 \times 10^{-10}$, $R_v = 1 \times 10^{-16}$.

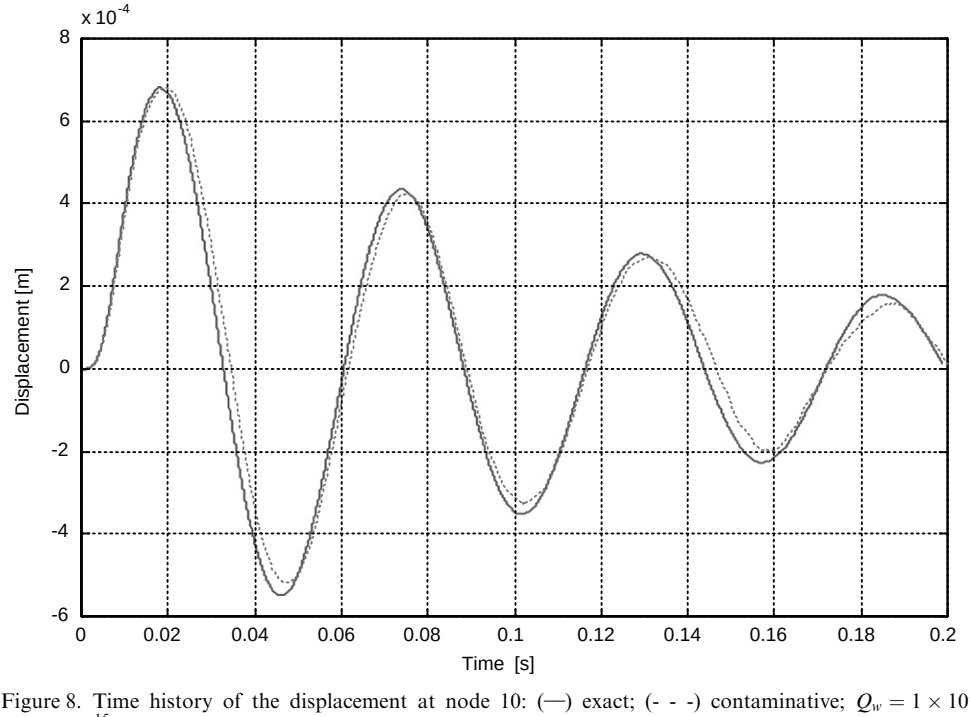

Figure 8. Time history of the displacement at node 10: (—) exact; (- - -) contaminative; $Q_w = 1 \times 10^{-9}$, $R_v = 1 \times 10^{-15}$.

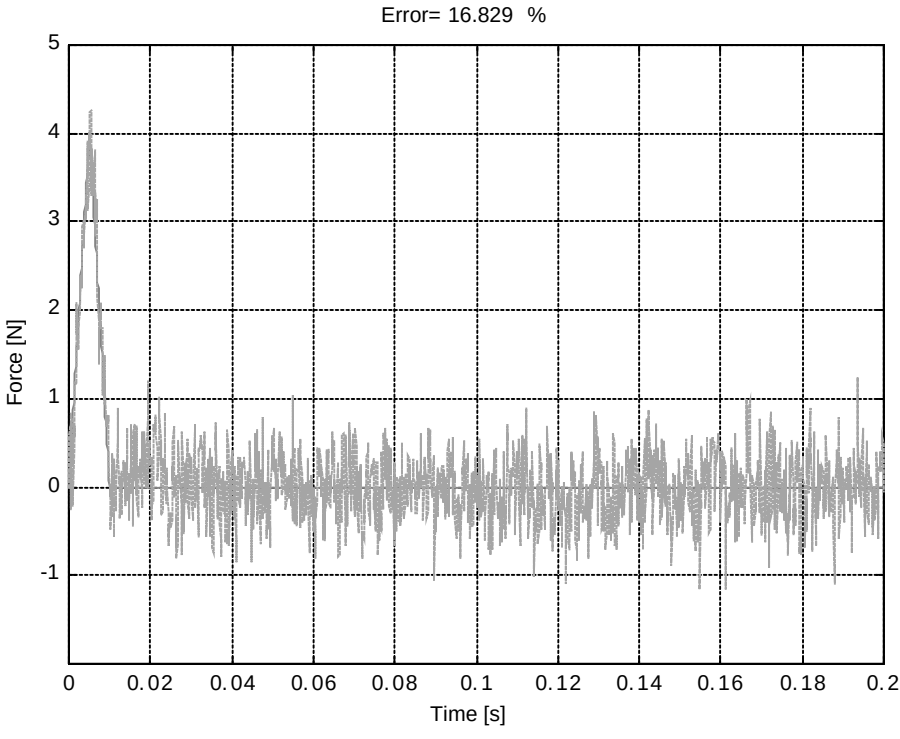

Figure 9. Time history of the triangular impulse at node 10: (—) exact; (- - -) estimated; $\gamma = 0{\cdot}52$, $Q_w = 1 \times 10^{-9}$, $R_v = 1 \times 10^{-15}$.

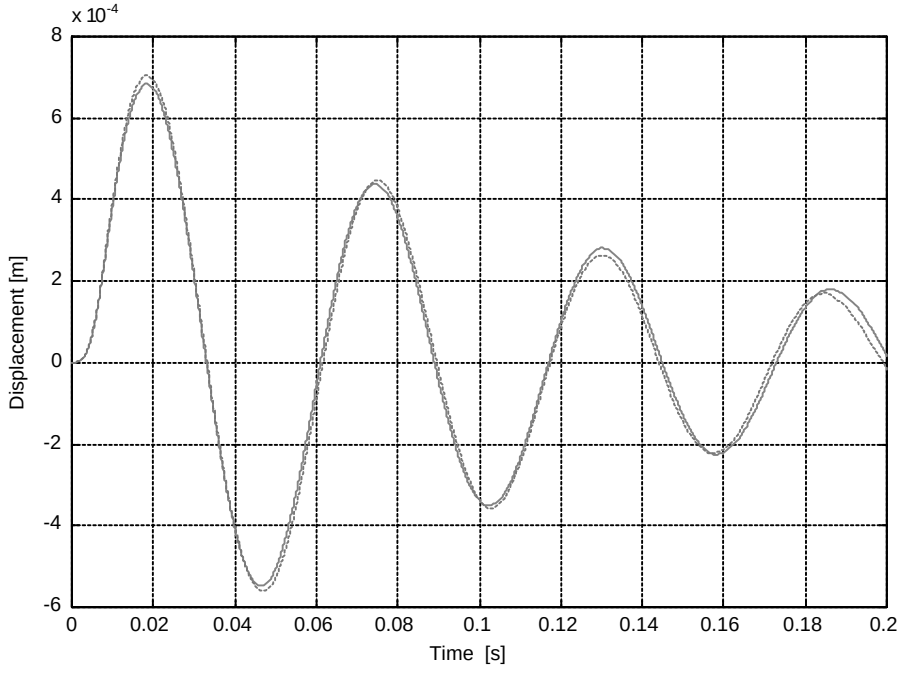

Figure 10. Time history of the displacement at node 10: (—) exact; (- - -) contaminative; $Q_w = 1 \times 10^{-10}$, $R_v = 1 \times 10^{-16}$.

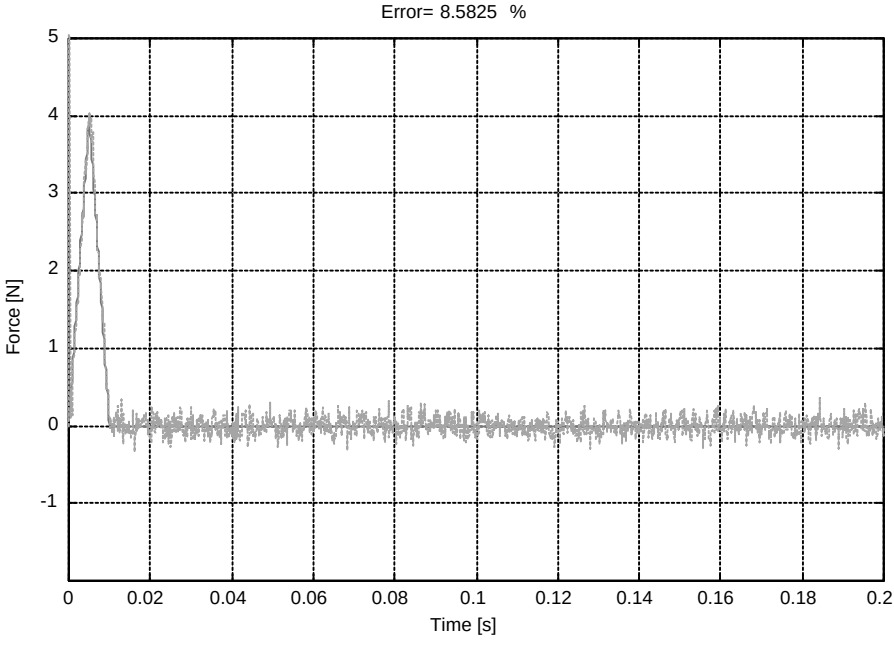

Figure 11. Time history of the triangular impulse at node 10: (—) exact; (- - -) estimated; $\gamma = 0{\cdot}52$, $Q_w = 1 \times 10^{-10}$, $R_v = 1 \times 10^{-16}$.

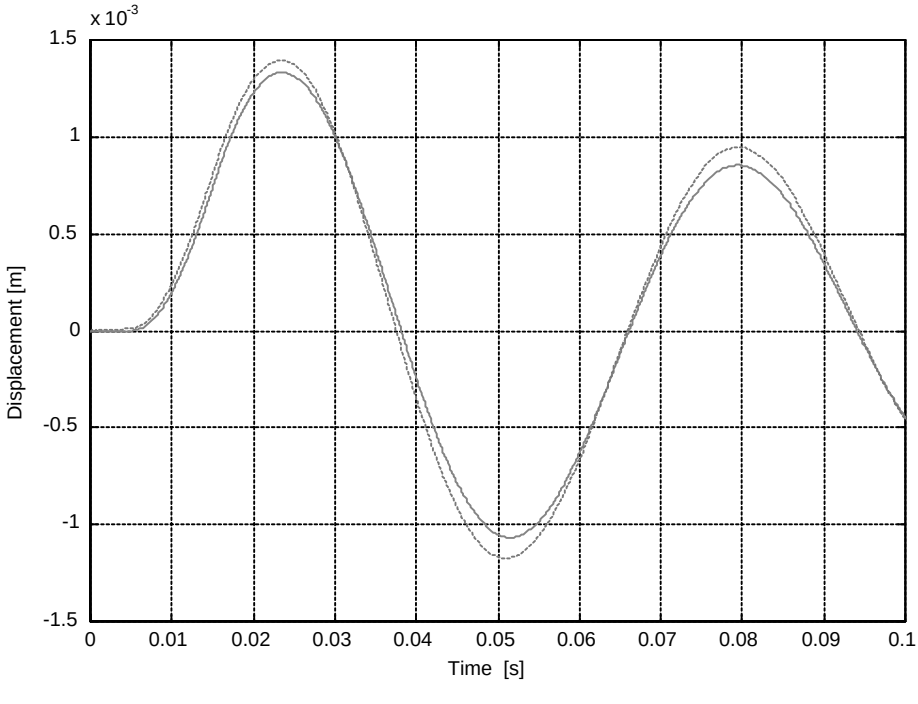

Figure 12. Time history of the displacement at node 10: (—) exact; (- - -) contaminative; $Q_w = 1 \times 10^{-9}$, $R_v = 1 \times 10^{-15}$.

3.3. ESTIMATION OF A RECTANGULAR IMPULSE

In the third demonstration, a rectangular impulse that acted on node 10 was assumed as

$$F_{10}(t) = 0\,(\mathrm{N}), \quad 0 \leqslant t \leqslant 0{\cdot}005\,(\mathrm{s}),$$

$$F_{10}(t) = 4\,(\mathrm{N}), \quad 0{\cdot}005 < t \leqslant 0{\cdot}015\,(\mathrm{s}),$$

$$F_{10}(t) = 0\,(\mathrm{N}), \quad t > 0{\cdot}015\,(\mathrm{s}).$$

The simulation parameters are the same as the previous test case. Figures 13 and 15 present the estimation results of the rectangular impulse at different levels of Q_w and R_v. From these figures, we can conclude that the present inverse method has an excellent tracking ability to identify input forces with abrupt changes.

3.4. ESTIMATION OF A SERIES OF IMPULSES

To examine the present inverse method in predicting complex input forces, a series of impulses that acted on node 10 was considered. The pattern of the series of impulses was expressed as

$$F_{10}(t) = 0\,(\mathrm{N}), \quad 0 \leqslant t \leqslant 0{\cdot}002\,(\mathrm{s}),$$

$$F_{10}(t) = 3(t - 0{\cdot}002)/(3 \times 10^{-3})\,(\mathrm{N}), \quad 0{\cdot}002 < t \leqslant 0{\cdot}005\,(\mathrm{s}),$$

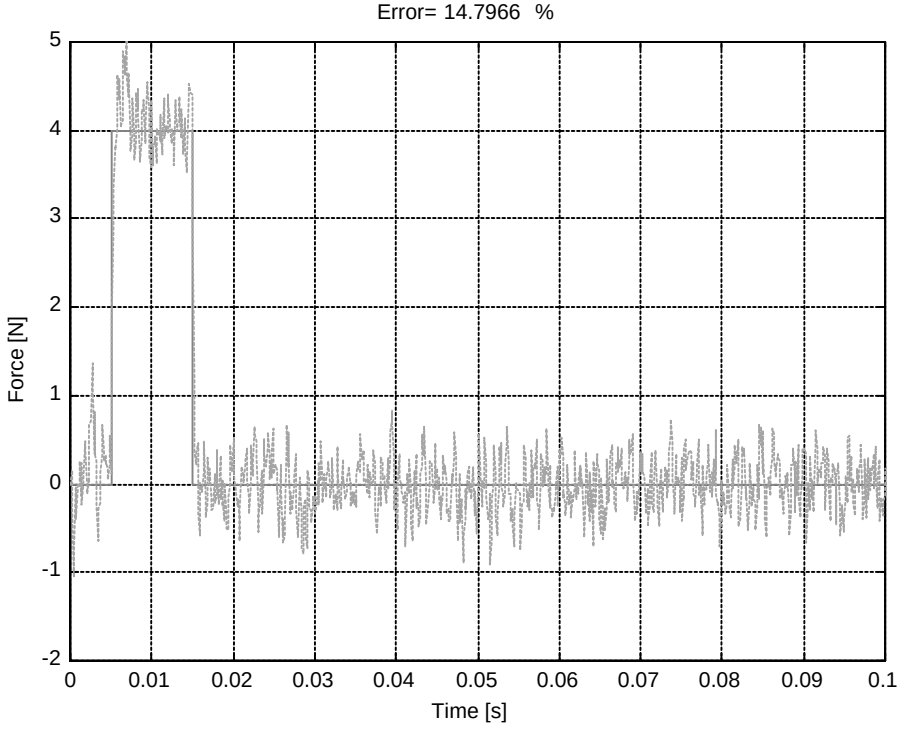

Figure 13. Time history of the rectangular impulse at node 10: (—) exact; (- - -) estimated; $\gamma = 0{\cdot}58$, $Q_w = 1 \times 10^{-9}$, $R_v = 1 \times 10^{-15}$.

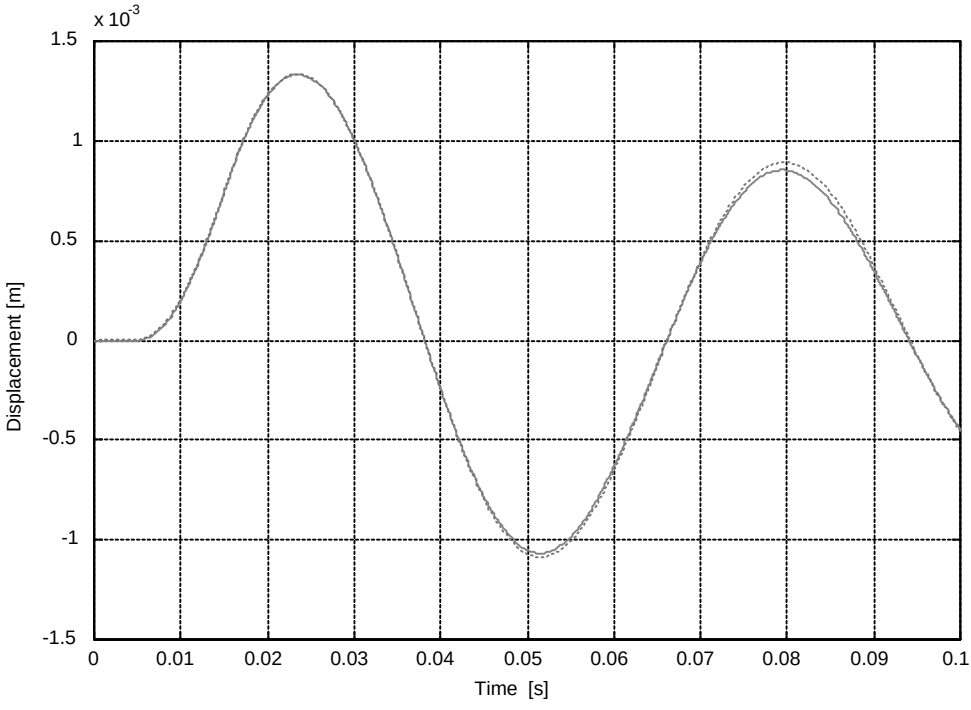

Figure 14. Time history of the displacement at node 10: (—) exact; (- - -) contaminative; $Q_w = 1 \times 10^{-10}$, $R_v = 1 \times 10^{-16}$.

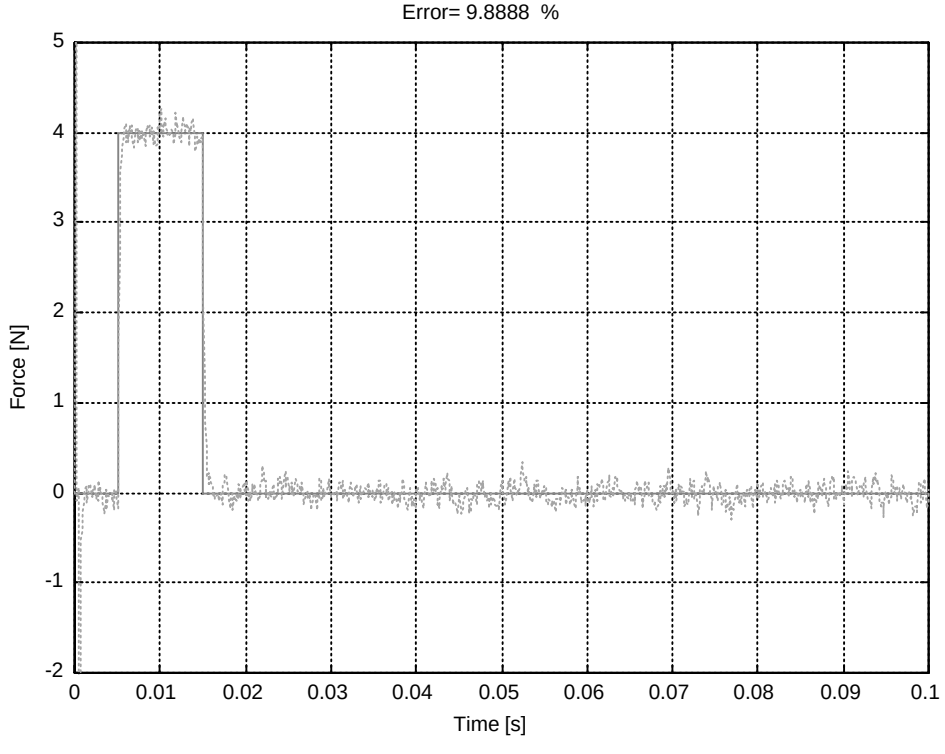

Figure 15. Time history of the rectangular impulse at node 10: (—) exact; (- - -) estimated; $\gamma = 0{\cdot}58$, $Q_w = 1 \times 10^{-10}$, $R_v = 1 \times 10^{-16}$.

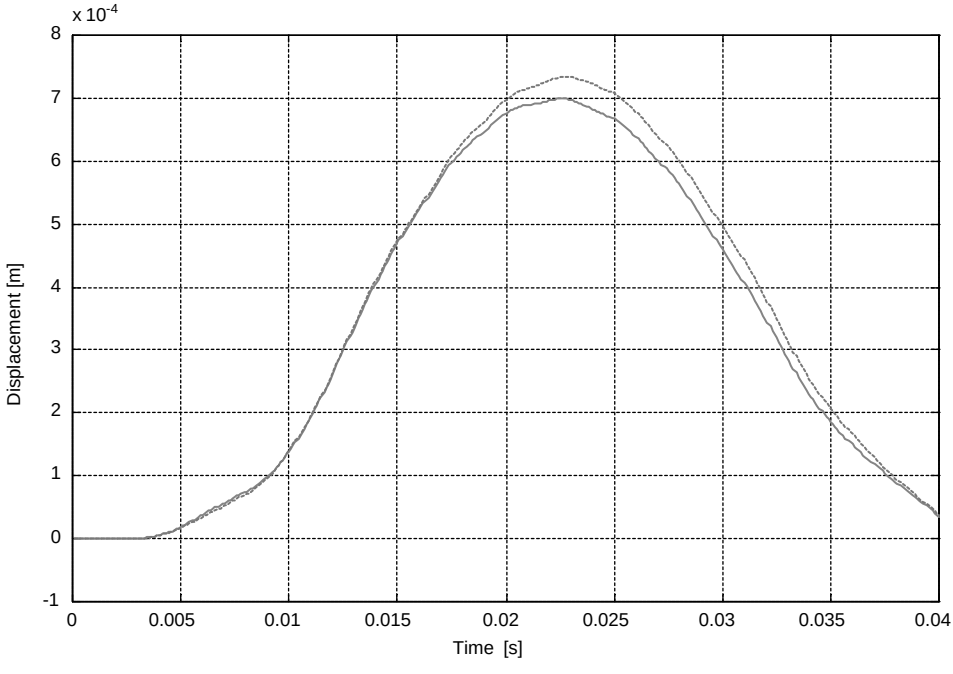

Figure 16. Time history of the displacement at node 10: (—) exact; (- - -) contaminative; $Q_w = 1 \times 10^{-9}$, $R_v = 1 \times 10^{-15}$.

$$F_{10}(t) = 0\,(\mathrm{N}), \quad 0{\cdot}005 < t \leqslant 0{\cdot}008\,(\mathrm{s}),$$

$$F_{10}(t) = 4\,(\mathrm{N}), \quad 0{\cdot}008 < t \leqslant 0{\cdot}012\,(\mathrm{s})$$

$$F_{10}(t) = 0\,(\mathrm{N}), \quad 0{\cdot}012 < t \leqslant 0{\cdot}015(\mathrm{s}),$$

$$F_{10}(t) = 3 \times \sin(\pi t/9{\cdot}52575)\,(\mathrm{N}), \quad 0{\cdot}015 < t \leqslant 0.030\,(\mathrm{s}),$$

$$F_{10}(t) = 0\,(\mathrm{N}), \quad 0{\cdot}030 < t \leqslant 0{\cdot}033\,(\mathrm{s}),$$

$$F_{10}(t) = 4(0{\cdot}038 - t)/(5 \times 10^{-3})\,(\mathrm{N}), \quad 0{\cdot}033 < t \leqslant 0{\cdot}038\,(\mathrm{s}),$$

$$F_{10}(t) = 0\,(\mathrm{N}), \quad t > 0{\cdot}038\,(\mathrm{s}).$$

The estimation results of the mixed impulses are presented in Figures 17 and 19. These results indicate that the estimation technique has superior performance in tracking complex unknown input forces.

3.5. ESTIMATION OF A RANDOM FORCE

Finally, we considered the estimation of a random force that acted on node 10. In the numerical experiment, the random force was generated by a signal generator as below:

$$F_{10}(t) = 20 \times \text{random signal}\,(\mathrm{N}).$$

The estimation result in Figure 21 reveals that the present inverse method provides a reliable tracking capability for the random force. Thus, we can conclude that the present

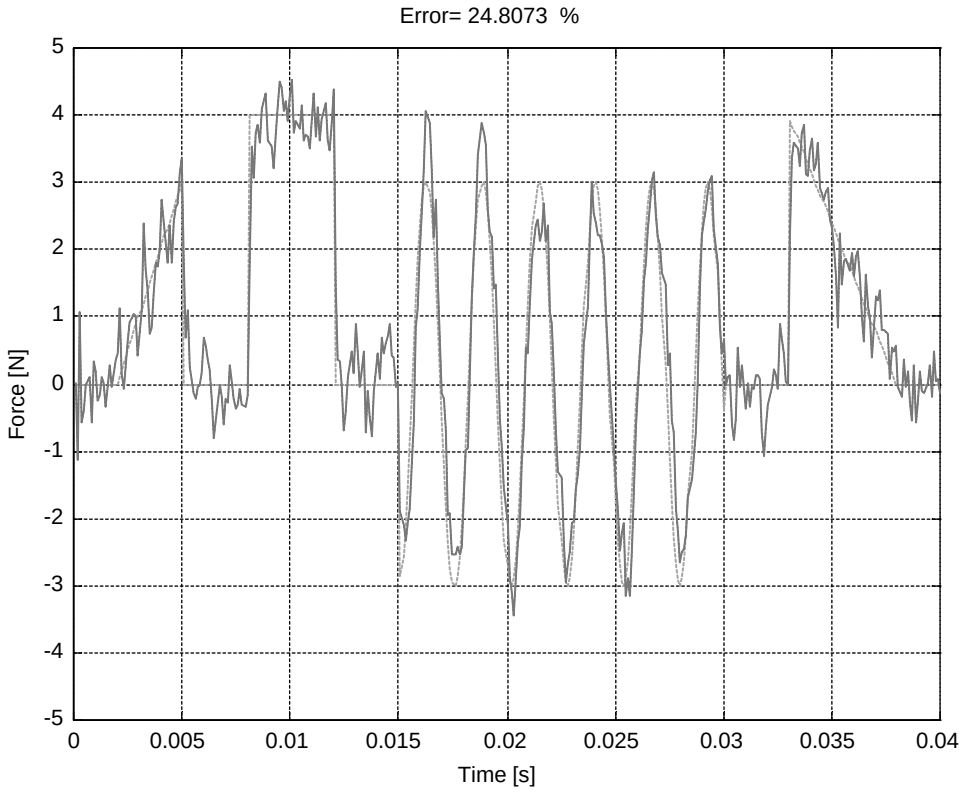

Figure 17. Time history of the series of impulses at node 10: (—) exact; (- - -) estimated; $\gamma = 0{\cdot}46$, $Q_w = 1 \times 10^{-9}$, $R_v = 1 \times 10^{-15}$.

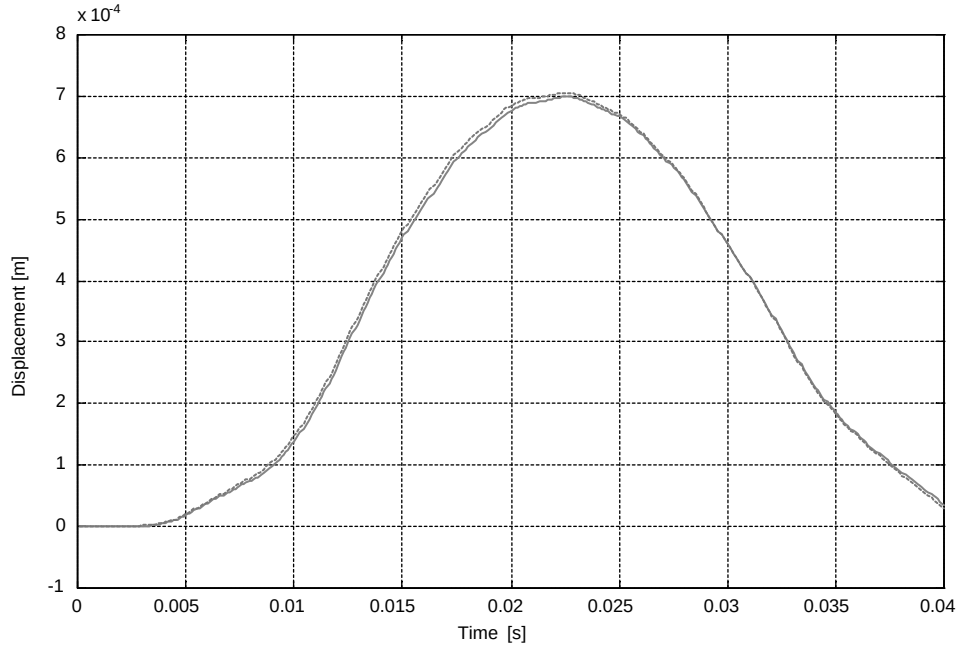

Figure 18. Time history of the displacement at node 10: (—) exact; (- - -) contaminative; $Q_w = 1 \times 10^{-10}$, $R_v = 1 \times 10^{-16}$.

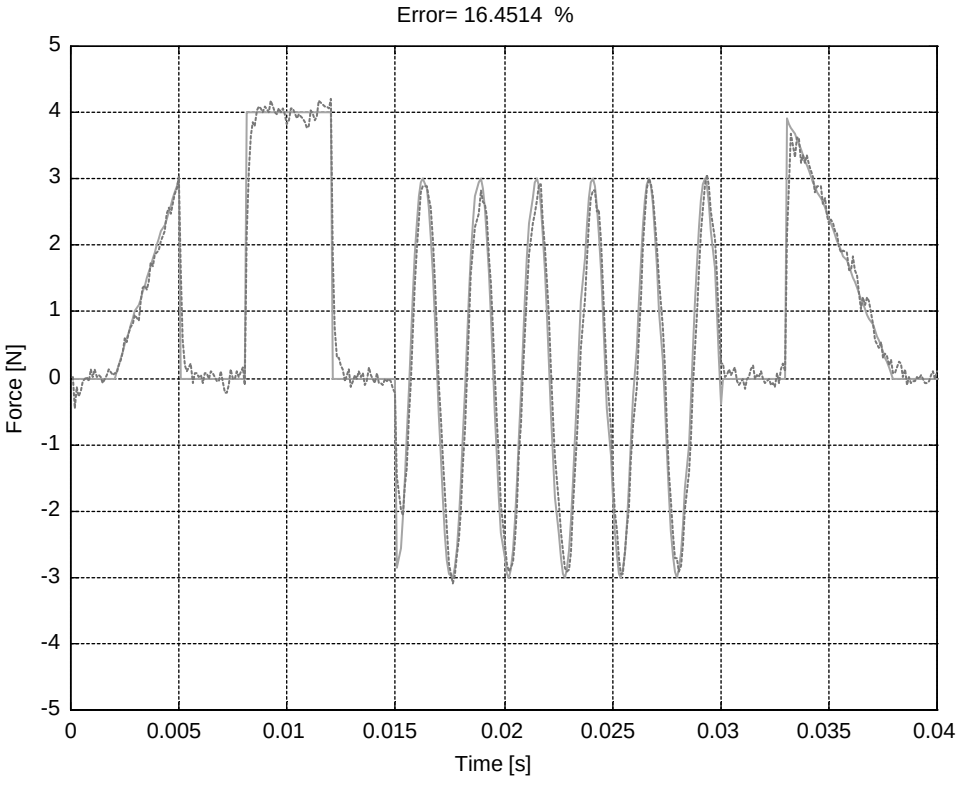

Figure 19. Time history of the series of impulses at node 10: (—) exact; (- - -) estimated; $\gamma = 0{\cdot}46$, $Q_w = 1 \times 10^{-10}$, $R_v = 1 \times 10^{-16}$.

estimation algorithm can be applied to beam structural systems in predicting unknown input forces in the real world.

4. DISCUSSIONS

(1) The Kalman filter is a recursive data-processing algorithm, such that all previous data, except the most recent, need not be kept in storage at the time where a new measurement is taken. Therefore, the present inverse method processes the measurements in an on-line form. On-line means that the unknown input forces at any time step can be estimated recursively from measurements taken at the same time step. In addition, the present scheme, with its recursive structure, can save a lot of memory and reduce the computational loads of computers.

(2) From the figures of the estimation results, we have found that there exists a time delay between the exact and the estimated input forces. It is well known that the cross-correlation function gives a measure of how much two signals in the time domain are "alike" with a certain delay between them [20]. From the evaluation of the cross-correlation function between the exact and the estimated input forces, a three-time-step delay was found. Therefore, before evaluating the errors of the estimation results, we have made time delay shifting treatments in time histories of the estimated input forces.

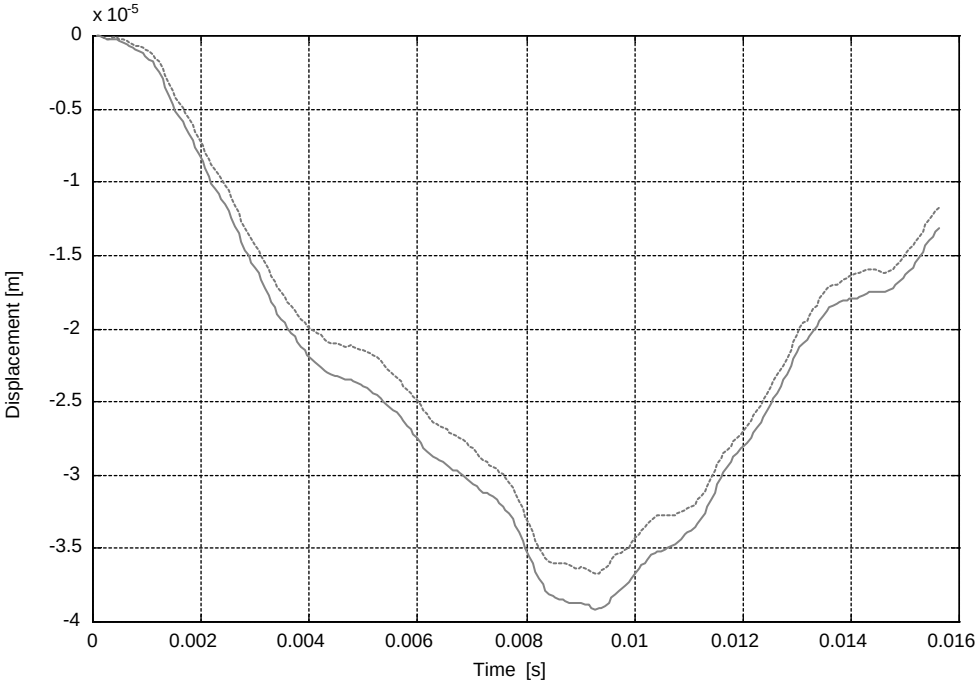

Figure 20. Time history of the displacement at node 10: (—) exact; (- - -) contaminative; $Q_w = 1 \times 10^{-9}$, $R_v = 1 \times 10^{-15}$.

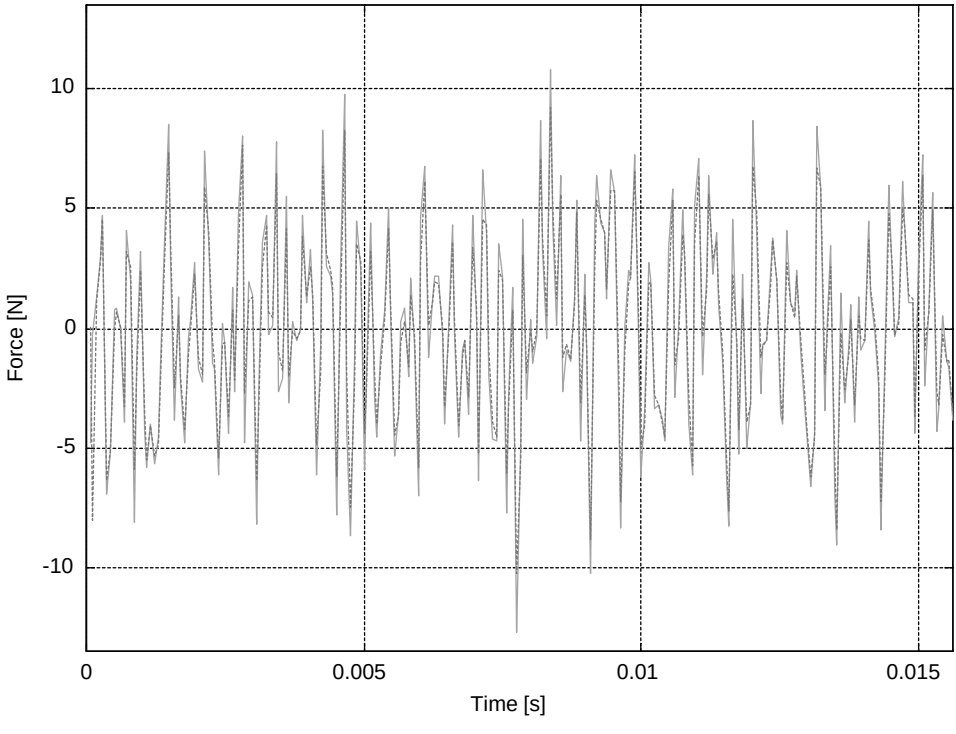

Figure 21. Time history of the random force at node 10: (—) exact; (- - -) estimated; $\gamma = 0{\cdot}16$, $Q_w = 1 \times 10^{-9}$, $R_v = 1 \times 10^{-15}$.

(3) Since $\mathbf{P} = P \times \mathbf{I}_{2n\times 2n}$ and $\mathbf{P}_b = P_b \times \mathbf{I}_{n\times n}$ are normally not known, the estimator is initialized with P and P_b as large numbers, such as 10^6 and 10^2 respectively. This has the effect of treating the errors in the initial estimation of the input forces as large. However, after a few time steps, the estimation results converge to their actual values rapidly. This shows that the present technique has the capability to correct the errors in the initial estimation.

(4) The estimation results of the input forces with high levels of Q_w and R_v have large fluctuations, as shown in Figures 5, 9, 13 and 17. The errors of the estimated input forces at different levels of Q_w and R_v are presented in Table 3. As these figures and table reveal, large process and measurement noises can cause degradation of estimation accuracy. However, the present inverse method can still track the unknown input forces where the large process and measurement noises are considered (Table 3).

(5) The estimation results of the two sinusoidal forces indicate that the present estimation algorithm is capable of dealing beam structural systems with multiple inputs and multiple outputs (MIMO).

5. CONCLUSIONS

This work has presented an on-line recursive inverse method to estimate the unknown input forces of beam structural systems. We used the FEM to construct the state equations of beam structures. The state-space analysis of the system is performed to employ the present input estimation algorithm. The feasibility of the present method was examined with the numerical experiments of a cantilever beam. The estimation results of all test cases show that the present approach can accurately estimate the periodic, impulsive and random excitation forces of beam structural systems. Results also indicate that the present technique is capable of handling noisy measurements. We have demonstrated the effectiveness of the present method in estimating input forces with time-varying and discontinuity. The random force estimation is useful to identify the excitation loads of beam structures frequently occurring in realistic environments. Future works of this study would address the problems of input forces estimations of two- and three-dimensional structural systems, and the applications in vibration control.

REFERENCES

1. K. K. Stevens 1987 *Proceedings of the 1987 SEM Spring Conference on Experimental Mechanics*, Houston, TX, U.S.A., 14–19. Force identification problems—an overview.
2. B. Hillary, D. J. Ewins 1984 *Proceedings of the Second IMAC*, Orlando, FL, U.S.A., 627–634. The use of strain gauges in force determination and frequency response function measurements.
3. H. Öry, H. Glaser, D. Holzdeppe 1986 *Proceedings of the Fourth IMAC*, Los Angeles, CA, U.S.A., 850-857. Quality of modal analysis and reconstruction of forcing functions based on measured output data.
4. D. Williams 1948 *Aeronautical Research Council*, Technical Report No. 2221. Dynamic loads in aeroplanes under given impulsive loads with particular reference to landing and gust loads on a large flying boat.
5. V. I. Bateman, T. G. Carne, D. L. Gregory, S. W. Attaway, H. R. Yoshimura 1991 *American Society of Mechanical Engineers Journal of Vibration and Acoustics* **113**, 192–200. Force reconstruction for impact tests.
6. J. F. Doyle 1984 *Experimental Mechanics* **24**, 265–270. Further developments in determining the dynamic contact law.

7. J. F. Doyle 1987 *Experimental Mechanics* **27**, 68–72. Determining the contact force during the transverse impact of plates.
8. J. F. Doyle 1993 *Experimental Mechanics* **33**, 64–69. Force identification from dynamic responses of a bimaterial beam.
9. M. T. Martin, J. F. Doyle 1996 *International Journal of Impact Engineering* **18**, 65–77. Impact force identification from wave propagation responses.
10. J. F. Doyle 1997 *Experimental Mechanics* **37**, 403–408. A wavelet deconvolution method for impact force identification.
11. J. E. Michaels and Y. H. Pao 1985 *Journal of the Acoustical Society of America* **77**, 2005–2011. The inverse source problem for an oblique force on an elastic plate.
12. C. D. Johnson 1998 *Shock and Vibration* **5**, 181-197. Identification of unknown, time-varying forces/moments in dynamics and vibration problems using a new approach to deconvolution.
13. C. H. Huang 2001 *Journal of Sound and Vibration* **242**, 749–765. An inverse non-linear force vibration problem of estimating the external forces in a damped system with time-dependent system.
14. C. K. Ma, P. C. Tuan, D. C. Lin and C. S. Liu 1998 *International Journal of Systems Science* **29**, 663–672. A study of an inverse method for the estimation of impulsive loads.
15. C. K. Ma, D. C. Lin 2000 *Inverse Problems in Engineering*, **8**, 511–528. Input forces estimation of a cantilever beam.
16. P. S. Maybeck 1979 *Stochastic Models, Estimation, and Control*. New York: Academic Press.
17. P. C. Tuan, C. C. Ji, L. W. Fong and W. T. Huang 1996 *Numerical Heat Transfer* B, **29**, 345–363. An input estimation approach to on-line two dimensional inverse heat conduction problems.
18. N. Kikuchi 1986 *Finite Element Methods in Mechanics*. Cambridge: Cambridge University Press.
19. G. Genaro, D. A. Rade 1998 *Proceedings of the 16th IMAC*, Santa Barbara, CA, USA, 124–129. Input force identification in the time domain.
20. H. Herlufsen 1984 *B&K Technical Review*, 199–251. Dual channel FFT analysis (part I).

APPENDIX A: NOMENCLATURE

$\mathbf{A}$	constant matrix
$\mathbf{B}$	constant matrix
$\mathbf{B}_s$	sensitivity matrices
$\mathbf{C}$	damping matrix
E	elastic modulus
$\mathbf{F}$	impulsive load vector (the unknown inputs to be estimated)
$\mathbf{H}$	measurement matrix
I	moment of inertia
$\mathbf{I}$	identity matrix
k	time (discretized)
$\mathbf{K}$	stiffness matrix
$\mathbf{K}_a$	Kalman gain
$\mathbf{K}_b$	correction gain
ℓ	length of the beam element
$\mathbf{M}$	mass matrix
$\mathbf{M}_s$	sensitivity matrices
$\mathbf{P}$	filter's error covariance matrix
$\mathbf{P}_b$	error covariance matrix
$\mathbf{Q}$	process noise covariance matrix
Q_w	scalar of process noise covariance
$\mathbf{R}$	measurement noise covariance matrix
R_v	measurement noise covariance
$\mathbf{S}$	innovation covariance
t	time (continuous)
t_f	final time
V	measurement noise vector

$\mathbf{W}$	process noise vector
$\mathbf{X}$	state vector
$\mathbf{Y}$	displacement vector
$\dot{\mathbf{Y}}$	velocity vector
$\ddot{\mathbf{Y}}$	acceleration vector
$\mathbf{Z}$	observation vector
γ	fading factor
$\mathbf{\Gamma}$	input matrix
δ	Kronecker delta
Δt	sampling time (interval)
ρ_s	mass per unit length of the beam
σ	standard deviation
$\mathbf{\Phi}$	state transition matrix

Superscripts

$\hat{}$	estimated
–	estimated by filter
T	transpose of matrix

Subscripts

i, j	indices